PHYSICAL REVIEW B VOLUME 51, NUMBER 16 15 APRIL 1995-II

Vacancy kinetics and sputtering of GaAs(110)

R. J. Pechman, X.-S. Wang, and J. H. Weaver
Department of Materials Science and Chemical Engineering, University of Minnesota, Minneapolis, Minnesota 55455
(Received 28 November 1994; revised manuscript received 16 January 1995)

Bombardment of GaAs(110) at $300 \leq T \leq 775$ K with Ar^+ ions at normal incidence creates surface-layer defects that generally span one or two unit cells, as shown by scanning tunneling microscopy. Vacancies produced in this way diffuse via thermal activation to form single-layer vacancy islands. The diffusion of divacancies favors $[1\bar{1}0]$ and accommodation at islands produces roughly isotropic islands. Modeling of growth showed an overall Arrhenius behavior for diffusion with an activation energy of 1.3 ± 0.2 eV. Investigations of the surface morphology during multilayer erosion revealed deviation from layer-by-layer removal with scaling exponents between 0.4 and 0.5 for $626 \leq T \leq 775$ K.

INTRODUCTION

Ions play an important role in processes involved with overlayer growth and material removal. For example, ion-assisted growth can lead to smoother films by creating defects that act as nucleation sites and by transferring energy to enhance diffusion. Material removal via reactive-ion or ion-assisted etching relies on energy provided to create chemically volatile species. Ions can also have adverse effects by creating disorder near the surface, as in vacancies in semiconductor materials. In such complex systems there are competing processes, and it is important to understand each so that processing conditions can be optimized.

In this paper, we focus on defects created on GaAs(110) by noble gas bombardment and vacancy migration under the influence of temperature and sustained ion impact. Vacancies can be created on a semiconductor surface by sputtering with ions at energies of a few hundred to a few thousand eV. When done at elevated temperature, it is possible to promote near-surface healing, and the defects can be characterized in terms of size and structure using atomic resolution scanning tunneling microscopy (STM). Vacancy kinetics can be extracted by relating surface morphology after erosion to vacancy migration and the formation of vacancy islands. In such circumstances, the results can be explained using some of the vocabulary of thin-film growth. Such parallels to growth have been developed recently for sputter erosion[1–5] and for spontaneous etching.[6–8]

Here the activation energy for diffusion of vacancies has been determined from the temperature-dependent size and density distribution of single-layer-deep vacancy islands. Denuded zone analysis indicates migration of divacancies along $[1\bar{1}0]$ and offers insight into the mechanism for vacancy motion. Extension of these investigations to high fluence resulted in multilayer erosion. Analysis of height profiles as a function of fluence and temperature shows that ideal layer-by-layer conditions could not be achieved. We attribute this to insufficient interlayer mass transport and, ultimately, the instability of GaAs against As desorption.

EXPERIMENT

The experiments were conducted in an ultrahigh-vacuum chamber equipped with a Park Scientific Instruments STM. The base pressure was $\sim 1 \times 10^{-10}$ Torr. Clean (110) surfaces were prepared by cleaving GaAs posts that were doped p type with Zn at $\sim 2 \times 10^{18}$ cm^{-3} and n type with Si at $\sim 1 \times 10^{17}$ cm^{-3}. Sputtering was done with a differentially pumped ion gun using high-purity Ar introduced via a precision leak valve. The gun was thoroughly degassed before every bombardment. Vacancy island nucleation studies involved sputtering with 300–500-eV Ar^+ at fluxes of $3-6 \times 10^{11}$ ions cm^{-2} s^{-1} at temperatures of 625–775 K. Multilayer erosion studies used 3000-eV Ar^+ at a flux of 1.9×10^{12} ions cm^{-2} s^{-1} at temperatures of 625–775 K. The pressure in the STM chamber did not exceed 6×10^{-9} Torr during bombardment. Temperatures were measured with a thermocouple near the sample base that was calibrated using an optical pyrometer. Quoted values were accurate to ± 20 K and reproducible to ± 10 K. This relatively large uncertainty reflects the fact that the samples were cleaved posts which had a range of shapes and overall profiles. The sample was cooled rapidly to room temperature after sputtering for STM experiments. Electrochemically etched tungsten tips were cleaned *in situ* by electron irradiation. Micrographs shown here represent occupied states images (As sublattice) acquired in a constant current mode with biases of 1.5–3.0 V. They were not corrected for thermal drift, and some show slight distortions. $[1\bar{1}0]$ runs from upper left to lower right in all images. The piezoelectric scanner was calibrated by comparing driftless atomic resolution images of GaAs(110) to the known lattice spacings and by measuring monatomic step heights on GaAs(110).

RESULTS AND DISCUSSION

Vacancy island nucleation and growth

Wang, Pechman, and Weaver[9] recently showed that Ar^+ ions having energies of 300–5000 eV induce surface

0163-1829/95/51(16)/10929(8)/$06.00 ©1995 The American Physical Society

damage on GaAs(110) that generally spans 1–5 unit cells where a unit cell is taken to be 4.00×5.65 Å^2. Room-temperature sputtering indicated that some material ejected from pits by ion impact remained on the surface as adatoms. The adatoms produced by sputtering at $600\leq T\leq775$ K were mobile, and thermal effects promoted local healing so that surface defects were well defined. For 300-eV ions, dual-bias imaging indicated that most impacts removed 1–4 atoms localized within a single row along [1$\bar{1}$0]. The yield of surface atoms removed per ion was constant when sputtering was done at normal incidence at $600\leq T\leq775$ K. The surface healing and the formation of vacancy islands appeared independent of the trajectory relative to the surface, even though effects due to trajectory and beam energy were clearly evident on the yield. Damage done deep within the sample was either healed or had no effect on the surface diffusivity of vacancies or vacancy complexes. Accordingly, we used Ar^+ at 300 eV and normal incidence to create the vacancies and small vacancy complexes whose behavior is quantified here. Figure 1 summarizes the results of analysis of these defects and shows that two-atom removal was the most likely under conditions where the damage was frozen and defect size could be estimated; defects more than five atoms in size generally spanned more than one row.

The fluxes corresponded to removal of $1-5\times10^{-3}$ monolayers (ML) per second. This ensured that a vacancy created within a diffusion length of a vacancy island would reach that island instead of encountering other vacancies to produce an island that was stable at the formation temperature. With increasing temperature, of course, the sampled area increased and island coarsening occurred. This is analogous to atom deposition on a surface where nucleation competes with growth in a way that depends on the proximity of the deposited atom to an existing island. Exposures were limited to the removal of ≤0.08 ML to ensure that the islands did not grow together.

Figure 2 shows images for surfaces sputtered with 300-eV Ar^+ at fixed fluence for $625\leq T\leq775$ K. The upper limit of temperature was dictated by the fact that

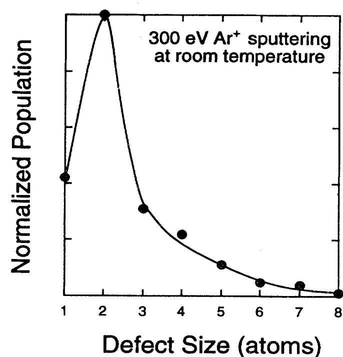

FIG. 1. Size distribution of defects formed by individual 300-eV Ar^+ impacts. Defects corresponding to two atoms are the dominant structures. For defects greater than about five atoms, the structures extend over two [1$\bar{1}$0] chains.

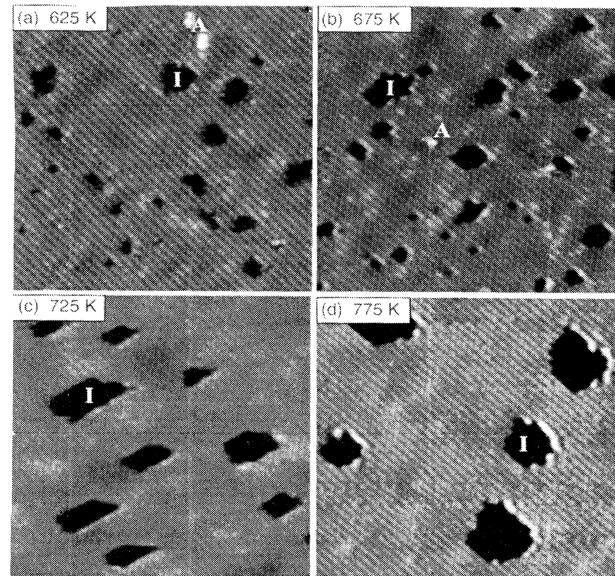

FIG. 2. 250×250-Å^2 images of GaAs(110) sputtered with 300-eV Ar^+ at 3×10^{11} ions cm^{-2} s^{-1} to remove ~0.05 ML. *I* denotes single-layer-deep vacancy islands, and *A* labels features associated with material ejected onto the surface.

As desorbs above 800 K, even without surface disorder induced by sputtering. Sputtering below 600 K produced surfaces that were dominated by structures comparable in size to those created by single-ion impacts because diffusion was insufficient to allow island formation. Areal analysis for each of the surfaces shown in Fig. 2 indicates the removal of about 0.05 ML with a yield that was nearly constant. Inspection reveals that single-layer-deep vacancy islands, *I*, were the dominant structures. The lateral dimension of these islands increased with temperature and their density decreased. Annealing for 5–15 min at the sputtering temperature did not alter the island density. Thus their motion on the surface was sufficiently sluggish to prevent them from joining with other islands. In addition, annealing to 775 K after sputtering at 625 and 675 K resulted in the same island density and size distribution as produced by sputtering at 775 K.

The STM images also revealed bright structures (*A*) that reflect material ejected onto the surface. Dual-bias imaging typically showed these bright spots in both polarities and that they extend ~5 Å. For room-temperature sputtering, the surface area covered by *A*-type features scaled with the pit area.[9] These features were stable against tip-induced displacement under the imaging conditions used here. They were observed less frequently at higher temperatures because they could recombine with vacancy islands or, for As_x species, they could desorb. Annealing after sputtering at lower temperatures reduced the density of *A*-type features. We found no evidence for regrowth features on the surface layer of the sort seen for Si(100),[1,5,7,8] or for adatom chains as reported for GaAs(110).[10]

Figure 3(a) shows an image obtained after sputtering of a region having two monatomic steps running along

[001]. The surface far from the steps was equivalent to that of Fig. 2(b), but the areal density of vacancies was much reduced close to the steps. Such denuded zones, labeled DZ, were absent along [1$\bar{1}$0] steps, as shown in Fig. 3(b). This indicates that divacancy diffusion is preferred along the zigzag chains of alternating Ga and As sites, perpendicular to [001]. The kinks along [001] steps represent sites where vacancies were accommodated. Divacancies created sufficiently close to the [001] step on the upper terrace were able to annihilate at the step. Those that diffused to the step from the lower terrace were not able to annihilate because this would involve atom dissociation from the step and transfer to the vacancy. These vacancies were reflected back onto the terrace under these low fluence conditions. Only at higher fluence did we observe the formation of extended vacancies along the step direction in the lower terrace, corresponding to creation of a double-height step. The larger kinks along the edge in Fig. 3(b) probably represent vacancy islands that coalesced with the step edge. The linear density of these kinks is equal to the linear density of vacancy islands along [1$\bar{1}$0] far from [1$\bar{1}$0] steps.

Figure 3(c) depicts the top layer of a GaAs(110) terrace with a single As vacancy (V_{As}), two GaAs divacancies (V_{GaAs}), and a vacancy island. The island is bounded by two GaAs [1$\bar{1}$0] chains. The one on the right is terminated by As atoms, while that on the left is terminated by Ga atoms. The top and bottom edges are regular [001] steps and the overall island is charge neutral. Atoms within the exposed second layer of GaAs are also shown. The images of Fig. 2 reveal such single-layer-deep islands, but with borders that are less regular because of kink sites and segments of ⟨112⟩-type steps. Dual-bias imaging and inspection of the atomic sites of the exposed second layer shows the Ga and As aspects of the [1$\bar{1}$0] and [001] edges.

Vacancy diffusion can be visualized from Fig. 3(c). For a V_{GaAs} unit like II or III, movement by one atomic site along [1$\bar{1}$0] will occur when a Ga or As atom jumps from one end of the vacancy to an equivalent site at the other end, as depicted by the dashed downward arrows, and discussed for GaAs(110) by Gwo, Smith, and Shih[11] and Lengel *et al.*[11] Motion of V_{GaAs} (or larger complexes contained within a zigzag row having an even number of

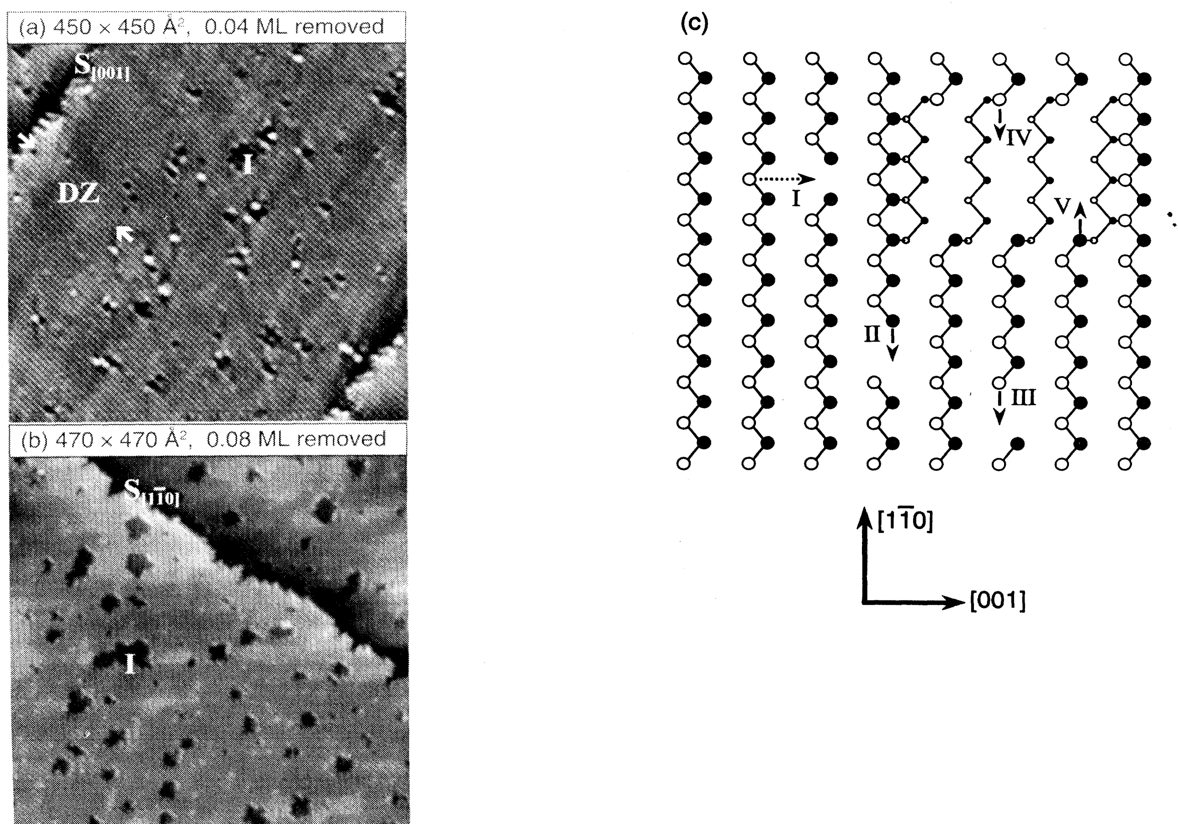

FIG. 3. (a) 450×450-Å^2 image showing a denuded zone (DZ) near a [001] step, labeled $S_{[001]}$. The island density is reduced near down-steps (upper left) but unaffected near up-steps (lower right). A typical vacancy island is indicated by *I*. (b) 470×470-Å^2 image of a surface sputtered to remove twice as much material as in (a). A monatomic [1$\bar{1}$0] step is seen, and no denuded zone exists. (c) Schematic representation of GaAs(110) with Ga atoms shown as filled circles and As atoms as open circles. Distinct vacancy sites are shown: a single As vacancy (V_{As}), two GaAs divacancies (V_{GaAs}), and a larger vacancy island. The zigzag row direction is indicated. Diffusion of V_{GaAs}-type defects was found to be highly anisotropic along [1$\bar{1}$0]. The arrows indicate that single atom hopping is the mechanism for net displacement.

missing atoms) can be accomplished by net hopping of As and Ga atoms along [1$\bar{1}$0]. The activation energy for such diffusion is dominated by the breaking of one surface bond and one backbond as the atom dissociates from one end of the vacancy. The divacancies depicted in Fig. 3(c) could be accommodated at the island such that II would cause elongation along [001] and III elongation along [1$\bar{1}$0]. The fact that the aspect ratio for the islands in Fig. 2 is approximately unity indicates accommodation at both types of island edges.

Gwo, Smith, and Shih[10] have assessed diffusion anisotropy of native vacancy complexes on purposely miscleaved GaAs(110) at 300 K. Multiple scanning of the same area revealed occasional vacancy-hopping events along [1$\bar{1}$0] and far fewer hops along [001] that led them to deduce an anisotropy in diffusion of $\sim 10^3$ in favor of motion along the zigzag rows. Ebert, Lagally, and Urban[12] found tunneling conditions under which they were able to move divacancies along the zigzag rows of GaP(110) with a STM tip at 300 K. Lengel *et al.*[11] performed a similar study concerning single As vacancy hopping events on GaAs(110). They found that V_{As} moved across zigzag rows, as depicted by the horizontal arrow in Fig. 3(c), under the influence of the tip. Such an event involves breaking of only one backbond and bond rotation of the surface bonds as the atom swings out of the surface plane and into the vacancy site.[11] The alternative pathway, diffusion of a single vacancy along [1$\bar{1}$0], is unlikely because an event that avoids an antisite defect must break at least one surface bond and a backbond somewhere along its path while overcoming a barrier to motion that is complicated by the presence of the opposite species [e.g., the Ga atoms on either end of the As vacancy in defect I in Fig. 3(c)]. Lengel *et al.* deduced activation energy barriers of ~ 1.5 and ~ 3.5 eV for these two channels. We have not observed tip-induced diffusion at 300 K, and we deliberately imaged at low bias to avoid tip effects. Tip-induced events are easily detected by discontinuities in successive line scans at the affected site, and by differences in successive images of the same area. We conclude that the tip did not play a significant role in activating the large number of vacancy hops needed to produce the observed vacancy islands.

Sputtering at low energy can create trivacancies in a single row. Motion for trivacancies along [1$\bar{1}$0] is complicated by the barrier just noted for single-atom vacancies. These immobile, odd-numbered vacancies can be converted to even-number structures via capture of a single-atom vacancy or capture of a surface adatom. Alternatively, a trivacancy can dissociate into a divacancy and a single-atom vacancy on an adjacent row, both of which can diffuse along their low-energy directions. In this case, the final thermodynamic state involves at net loss of one surface bond.

The shape of a vacancy island will change as atoms at the perimeter break away, diffuse on the island floor, and are rebonded. Dissociation events like IV and V in Fig. 3(c) are governed by the same bond-breaking energies as for V_{GaAs} diffusion. Accommodation of an atom diffusing on an island floor must be limited to chemically favorable sites. The result of atom dissociation from edges and reaccommodation at favorable sites is a reduction in kinks at vacancy island borders, leading to a smooth appearance of edges.

The activation energy for diffusion, E_d, can be calculated from analysis of images like those of Fig. 2, where island densities can be determined directly. The area associated with each island defines an average separation between islands. The problem of determining E_d is analogous to determining activation energies for diffusion of adatoms and clusters during growth. Mo *et al.*[13] have proposed a model that takes an atomistic view, first counting the number of sites visited by a diffusing species after H hops of length a. When H is large and diffusion is highly anisotropic, the number of distinct sites visited is $\sim H^{-1/2}$. The island density N is important when calculating the number of hops needed to find an existing island. From this a nucleation rate dN/dt can be deduced that depends on diffusivity D, deposition rate R, and total coverage θ. Integration then gives $N^7 = 7R^2\theta D^2 a^4$. Since N is determined by counting the islands, D can be calculated. This applies only to systems with highly anisotropic diffusion, low coverages where island radii are much smaller than the average island separation, and for low deposition rates where diffusing species interrogate large areas before encountering other migrating species. The low-Ar^+ fluxes and fluences used for our pit nucleation studies and the results of denuded zone analysis ensured that these conditions were satisfied.

The calculation of an activation energy for diffusion requires that there is a single dominant pathway, so that competing rate processes can be neglected. In our case, the rate processes can be categorized as vacancy creation, annihilation, migration, and nucleation and growth. Vacancy creation is governed by Ar^+ impact events, and removal was found to be constant with temperature at the fluxes used here. Vacancy annihilation occurs when adatoms fill vacancies. For $625 \le T \le 775$ K, the adatoms could combine with vacancies and were not often observed. Such events must have occurred locally as part of the healing of disorder at impact sites, and their time scale must have been much shorter than that for vacancy migration. By limiting the amount of material removed, the effects of growth rate were minimized, and it is reasonable to expect that vacancy accommodation at island edges was not sensitive to temperature in the range of interest. Finally, the rate of island nucleation was certainly temperature dependent and tied to island density. This was exploited to calculate the activation energy for divacancy migration. Thus the conditions of low flux ensured that vacancy diffusion was the rate process that was important in these nucleation studies.

Figure 4 summarizes the results of calculating D from the island density for surfaces sputtered at 625, 675, 725, and 775 K. Each datum point represents D averaged over vacancy island densities for fluences that resulted in 1–8 % vacancy coverage. Hundreds of vacancy islands were counted for each experiment, with at least four experiments done at different fluences for each of the four temperatures studied. Linearity of the fit indicates that vacancy diffusion follows an Arrhenius behavior. The slope gives $\Delta E_d = 1.3 \pm 0.2$ eV,[14] where the uncertainty

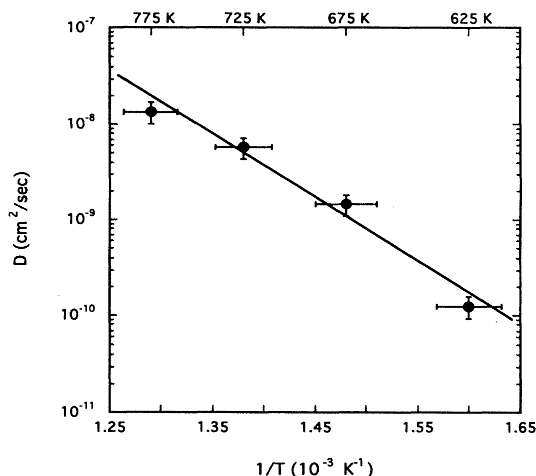

FIG. 4. Plot of vacancy diffusivity vs $1/T$. The slope of the straight line fit gives the activation energy for diffusion, $E_d = 1.3 \pm 0.2$ eV. Vertical error bars account for flux variations during bombardment.

reflects variations in ion flux during bombardment.[9] This activation energy reflects divacancy motion along zigzag chains. Single vacancies that were created contributed to island growth, but the fact that they were rarely observed after sputtering at elevated temperature indicates that they were sufficiently mobile to be accommodated at vacancy islands. While incorporation into an existing island would not affect the island density, it would alter the diffusion characteristics of the island, as noted above. For example, capture of a single vacancy by a divacancy would immobilize the complex and prevent the divacancy from sampling its full diffusion length. The net effect of such processes would be an increase in island density. The measured value for E_d would then be higher than it should be for simple divacancy diffusion. We estimate the slope of the Arrhenius plot would give a higher value for E_d by ~ 0.1 eV if the presence of single vacancies led to an increase in island density by 20%. This was deduced by rescaling the original island density data to reflect a 20% reduction and then recalculating D.

Multilayer erosion

The above has focused on vacancy islands in the top layer. With continued material removal, top layer islands grow and coalesce and additional islands can be produced in the exposed layer before original layers are completely eroded. As the surface morphology evolves, vacancy accommodation at upper and lower steps becomes increasingly important in determining pit shapes and the probability for interlayer mass transport.

Wang, Pechman, and Weaver[9] have shown that the sputtering yield for normal-incidence bombardment of GaAs(110) depends weakly on ion energy because the probability for channeling increases with energy. However, the vacancy size produced by individual ions averages 4–6 atoms at 3000 eV instead of 2–4 atoms for 300 eV. In multilayer erosion studies, we used 3000-eV ions and higher fluxes to minimize exposure times and main chamber pressure. The total amount of material removed was determined by scaling the sputter yield with the total ion exposure, again expressing the value in monolayer equivalents of GaAs(110). These values were checked against areal analysis of exposed layers for lower fluences where the original surface could be identified.

Figure 5 shows the surface morphology after removal of 0.9 and 9.5 ML at 725 K. It is clear from the images that erosion proceeds in a simultaneous multilayer fashion with the probability of sputter removal from a particular layer governed by the fractional area exposed. In general, these surfaces are comprised of a main layer M, remnant islands R, and vacancy islands I. The total number of layers reflects the effectiveness of interlayer transfer, a temperature-dependent quality. The remnant structures appear in stacks as more material is removed

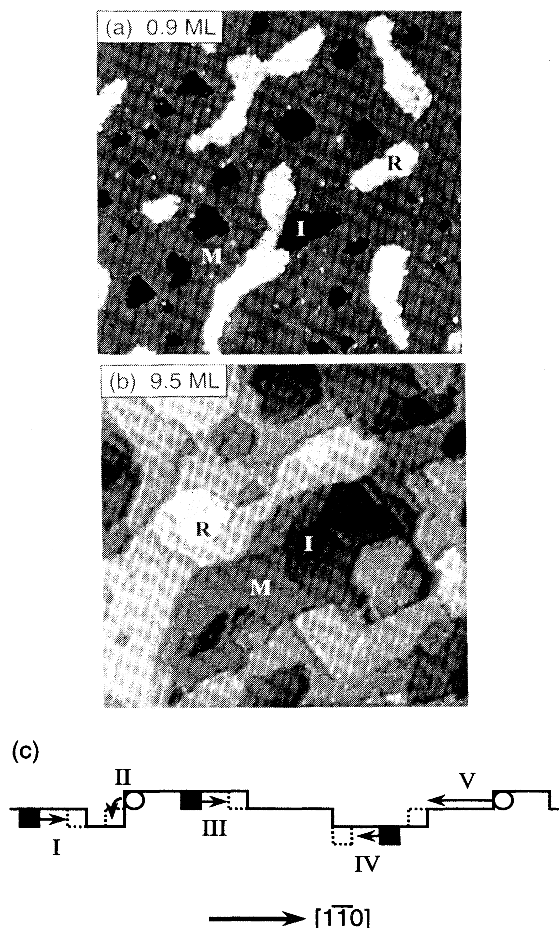

FIG. 5. 800×800-Å^2 images of GaAs(110) sputtered with 3000-eV Ar^+ at 1.9×10^{12} ions cm^{-2} s^{-1} at 725 K to remove (a) 0.9 ML and (b) 9.5 ML. Each surface is comprised of a main layer (M), remnant layers (R), and vacancy islands (I). Three layers are exposed in (a), whereas at least eight layers are exposed in (b). (c) Surface profile during multilayer erosion depicting possible vacancy accommodation and annihilation events.

and the step height between layers is generally one layer. The single-layer vacancy islands also appear in stacks as more material is removed. Figure 5(c) represents a general height profile after multilayer erosion. The horizontal axis is the fast diffusion direction for divacancies and possible vacancy accommodation mechanisms are indicated by I–V. In I, a vacancy in the main layer diffuses to a vacancy island and is accommodated. In II, a vacancy island abuts a portion of a remnant island where an atom dissociates from the upper terrace and is transported into the vacancy island. This interlayer vacancy diffusion via atom transfer reduces the root mean square surface roughness. In III, a vacancy in a remnant island diffuses to a single-height [001] step and reduces the size of the remnant. In IV, a next-layer vacancy migrates to an edge to form a double-height step. In V, an adatom liberated from a remnant island is accommodated at a favorable site of a step edge. This interlayer atom diffusion also reduces surface roughness. The shapes and distributions of the structures on eroded surfaces offers insight into the importance of these vacancy accommodation and interlayer mass transport phenomena.

In Fig. 5(a) there is no preferred alignment of the vacancy islands relative to the substrate crystallographic directions, and the islands have aspect ratios that are roughly 1:1. This indicates vacancy accommodation at both local [001] and $[1\bar{1}0]$ steps. The remnant islands in Fig. 5(a) do show elongation, but there is no preferential alignment because the island shape reflects vacancy coalescence. Remnant structures are formed when two isotropic vacancy islands meet, grow, and engulf other vacancy islands. Other growing vacancy islands are more likely to meet this large elongated one along the extended edge. If coalescence happens near an end point, the vacancy island will form a C shape that may meet itself at the ends, forming an elongated remnant island. The vacancy and remnant islands are bordered by irregular edges made up of segments of $[1\bar{1}0]$ and [001] steps. The $[1\bar{1}0]$ segments tend to be atomically straight over a few to several tens of Å, while the [001] steps are more kinked. This reflects the weaker interaction between adjacent chains compared to atoms in the same chain, as well as the higher probability for divacancy annihilation at [001] steps. Occasionally, double-height steps are formed at the junction of a vacancy island and remnant island [center of Fig. 5(a)]. In all cases, the double-height step segment roughly follows $[1\bar{1}0]$ or $\langle 112 \rangle$. Double-height steps along these directions form {111} microfacets. This is favorable since GaAs(111) reconstructs with a two-times periodicity to reduce the number of dangling bonds at a double-height edge. Such microfaceting was also observed following spontaneous etching of GaAs(110) with Br_2 and Cl_2.[15]

Figures 5(a) and 5(b) show that the average height deviation from the main layer increased with material removal at 725 K. Studies of multilayer sputtering at 625, 675, and 775 K showed the same trend. A measure of roughening can be obtained by defining an interface width $\langle H \rangle = [\langle h^2(x) \rangle - \langle h(x) \rangle^2]^{1/2}$, where $h(x)$ is the height at position x and $\langle \ \rangle$ denotes the average over the measured area. Here interface widths were calculated as a function of total material removed for the different temperatures of sputtering. When measured along a particular dimension, $\langle H \rangle$ showed no directional dependence, so that the roughness was independent on the choice of axis. This quantifies the observation above that there was no preferred shape or orientation for pits and islands formed during erosion.

Figure 6 plots the temperature dependence of the interface width versus material removed for surfaces sputtered at 625, 675, 725, and 775 K. Fewer data points were available for surfaces sputtered at 625 and 675 K since significant roughness for high fluences resulted in structures that were difficult to probe with a STM tip (deep and narrow). The slope of the linear best fit for each data set decreases from 0.5 at 625 K to 0.4 at 775 K. This is consistent with a 'growth' law whereby the interface width increases with time as $\langle H \rangle \propto t^{\beta}$ during deposition at constant flux, and the growth exponent β depends on temperature. Thus Fig. 6 reflects the dependence of the scaling exponent β on temperature for multilayer erosion.

Discussions of the growth exponent and its temperature dependence[16–19] show that $\beta = 0.5$ corresponds to a situation where there is no net mass transport between layers, and the morphology is statistically consistent with an ideal hit and stick picture. With increasing temperature, β decreases and there is a transition temperature at which it goes to 0, reflecting a steady state characterized by layer-by-layer growth and an interface width that is independent of time. β increases again above the roughening temperature because the adatom sticking probability decreases, the effects of thermal desorption cannot be ignored, and the growth front is roughened.[18,20]

From Fig. 6, it is clear that the erosion studied here for GaAs(110) occurs below the transition temperature since

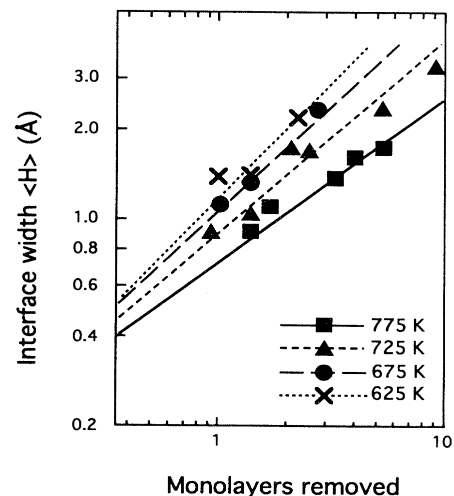

FIG. 6. Log-log plot of the interface width, $\langle H \rangle$, vs total amount of material removed for sputtering between 625 and 775 K. The errors involved are represented by the size of the symbols. The slope of each line gives the scaling exponent β at the corresponding temperature. β decreases slightly from 0.5 at 625 K to 0.4 at 775 K.

β did not reach a value near 0 and ideal layer-by-layer material removal was not observed. Erosion analogous to the roughening transition of growth occurs at ~ 800 K, corresponding to thermal desorption of As as As_x.[21] Accordingly, conditions where ideal layer-by-layer sputtering occurs cannot be realized. It should be noted that the behavior of β with time is asymptotic, and quantitation may require the removal of many tens of monolayers to obtain an accurate value. However, roughening observed here occurred sufficiently fast to determine the trend of β with temperature. Additional information about roughening during erosion can be obtained by tracking step density with temperature and fluence. Such analyses and the implication for quantitative understanding of physical erosion of GaAs will be described in detail elsewhere.[22]

Figure 7 shows STM images of surfaces sputtered to remove 1.5 ML at $625 \leq T \leq 775$ K. At 625 K, six layers are visible and the range of lateral continuity is small; at 775 K, four layers are visible and the terraces are large, indicating increased intralayer and interlayer migration at higher temperature. Inspection reveals structure with relatively small lateral dimensions and little change from 625 to 675 K. More noticeable lateral smoothing occurred at 725 and 775 K, although mathematical analysis shows that the scaling exponent changed only from 0.5 to 0.4 (Fig. 6), which indicates that interlayer mass transport is much more difficult than same-layer diffusion. Indeed, the interface width increases with time in an unbounded fashion during erosion.

The lateral dimension of structures after erosion reflects the details of lateral diffusion. Inspection of the images indicates that a main layer vacancy created on the surface in Fig. 7(d) would need to travel ~ 10 times farther to find a suitable accommodation site than for a main layer vacancy on the surface in Fig. 7(a). From Fig. 4, divacancy diffusivity is ~ 100 times larger at 775 K for Fig. 7(d) than at 625 K for Fig. 7(a). The diffusion lengths $x = \sqrt{D t}$ then differ by a factor of 10 for the same time. Thus the average lateral size correlates well with the lateral diffusivity, and the ranges of motion for vacancies governed by terrace sizes and by diffusion lengths scale equally with temperature. However, this does not account for the reduced roughness seen at the higher temperatures.

To understand the role of interlayer mass transport in reducing the surface roughness, we refer back to Fig. 5(c). Events like II and V constitute interlayer diffusion of vacancies and liberated atoms and decrease the interface width. Structure IV represents a vacancy created within an island. The size of the vacancy island will scale with temperature, as does the diffusion length. Moreover, the vacancy will be reflected back into the island floor when accommodation at the boundaries is not possible. Each time the vacancy reaches an edge there is a chance for an interlayer diffusion event like that depicted as II of Fig. 5(c). The fact that island boundary sampling rates are roughly independent of temperature indicates that interface smoothing is due to the activation barrier to interlayer diffusion events and not a reduction in the frequency factor (i.e., number of attempts) at lower temperatures.

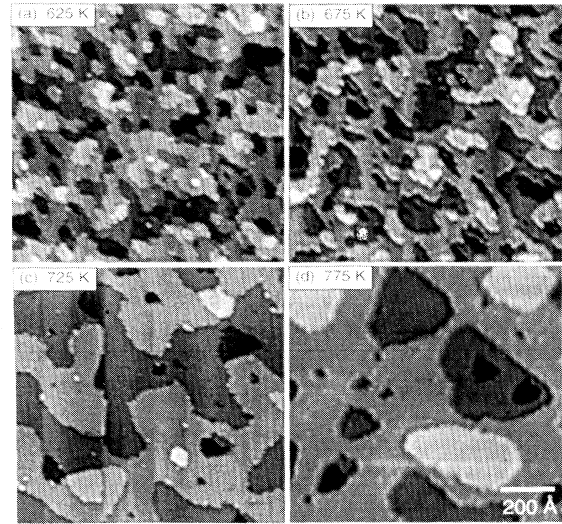

FIG. 7. 800×800-Å^2 STM images of GaAs(110) sputtered with 3000-eV Ar^+ at 1.9×10^{12} ions cm^{-2} s^{-1} to remove ~ 1.5 ML. The morphology appears much smoother for the surfaces sputtered at higher temperatures, although the interface width grows in an unbounded fashion due to ineffective mass transport between layers.

In addition to the mechanism of interlayer vacancy motion, events like V in Fig. 5(c) could occur to reduce the interface width. Such events represent atom dissociation from a remnant structure. The atom may then interrogate the surface to find a chemically favorable site at a remnant island or at a vacancy island. An encounter with a vacancy island would result in interlayer diffusion if the mobile atom hopped down at the island boundary and was accommodated. In principle, the diffusing adatom could encounter another liberated adatom and nucleate a separate island or, for the case of volatile As_x moieties, desorb. Such processes appear unlikely, since we have not observed small islands or detected a temperature dependence in the sputtering yield that would suggest significant desorption of As at higher temperature. Moreover, we have annealed surfaces like those shown in Fig. 7 to their respective sputtering temperatures for 5–10 min and observed no noticeable change in the size of remnant or vacancy islands or in surface roughness. This indicates that dissociation events like process V in Fig. 5(c) are not important for net interlayer mass transport, and cannot exclusively account for the reduction of interface width with temperature. We conclude that the unbounded surface roughening correlates to the difficulty of interlayer vacancy diffusion relative to the in-plane migration of these vacancies.

CONCLUSIONS

This paper has focused on the morphology of GaAs(110) under low- and medium-energy Ar^+ bombardment. STM analysis of vacancy island nucleation has shown an Arrhenius behavior for vacancy diffusion

with an activation energy for divacancy diffusion of 1.3±0.2 eV. Multilayer erosion studies revealed that sputtering leads to surface roughening below 775 K. Coverage- and temperature-dependent measurements of the interface width after bombardment showed ineffective mass transport between layers. It will be interesting to extend these studies to include ion enhanced growth and etching to gain insight into more complicated materials processing problems.

ACKNOWLEDGMENTS

This work was supported by the Army Research Office. The authors gratefully acknowledge discussions with D. Rioux, C. M. Aldao, D. W. Owens, and P. J. Benning.

---

[1] P. Bedrossian, J. E. Houston, J. Y. Tsao, E. Chason, and S. T. Picraux, Phys. Rev. Lett. **67**, 124 (1991); P. Bedrossian, Surf. Sci. **301**, 223 (1994).

[2] S. Gauthier, Y. Samson, J. C. Girard, S. Rousset, and J. Klein, J. Vac. Sci. Technol. B **12**, 1754 (1994).

[3] T. Michely and G. Comsa, Nucl. Instrum. Methods Phys. Res. Sect. B **82**, 207 (1993).

[4] J. C. Girard, Y. Samson, S. Gauthier, S. Rousset, and J. Klein, Surf. Sci. **302**, 73 (1994).

[5] H. J. W. Zandvliet, H. B. Elswijk, E. J. van Loenen, and I. S. T. Tsong, Phys. Rev. B **46**, 7581 (1992).

[6] J. C. Patrin, Y. Z. Li, M. Chander, and J. H. Weaver, Appl. Phys. Lett. **62**, 1277 (1993).

[7] D. Rioux, R. J. Pechman, M. Chander, and J. H. Weaver, Phys. Rev. B **50**, 4430 (1994).

[8] M. Chander, Y. Z. Li, J. C. Patrin, and J. H. Weaver, Phys. Rev. B **47**, 13 035 (1993).

[9] X.-S. Wang, R. J. Pechman, and J. H. Weaver, Appl. Phys. Lett. **65**, 2818 (1994); (unpublished).

[10] S. Gwo, A. R. Smith, and C. K. Shih, J. Vac. Sci. Technol. A **11**, 1644 (1993).

[11] G. Lengel, M. Weimer, J. Gryko, and R. E. Allen, J. Vac. Sci. Technol. A **12**, 1855 (1994).

[12] P. Ebert, M. G. Lagally, and K. Urban, Phys. Rev. Lett. **70**, 1437 (1993).

[13] Y.-W. Mo, J. Kleiner, M. B. Webb, and M. G. Lagally, Phys. Rev. Lett. **66**, 1998 (1991).

[14] This value is lower than the typical value of ~1.7 eV reported for bulk diffusion of Ga vacancies, consistent with the fact that the diffusion at surfaces is more facile than in the bulk. See T. Y. Tan, U. Gösele, and S. Yu, Crit. Rev. Solid State Mater. Sci. **17**, 47 (1991); D. E. Bliss, W. Walukiewicz, and E. E. Haller, J. Electron. Mater. **22**, 1401 (1993); and J.-L. Rouviere, Y. Kim, J. Cunningham, J. A. Rentschler, A. Bourret, and A. Ourmazd, Phys. Rev. Lett. **68**, 2798 (1992).

[15] J. C. Patrin and J. H. Weaver, Phys. Rev. B **48**, 17 913 (1993).

[16] M. G. Lagally, R. Kariotis, B. S. Swartzentruber, and Y.-W. Mo, Ultramicroscopy **31**, 87 (1989).

[17] R. Kariotis and M. G. Lagally, J. Vac. Sci. Technol. B **7**, 269 (1989).

[18] Z. Zhang, J. Detch, and H. Metiu, Phys. Rev. B **48**, 4972 (1993).

[19] Z.-W. Lai and S. Das Sarma, Phys. Rev. Lett. **66**, 2348 (1991).

[20] Y.-W. Mo, R. Kariotis, D. E. Savage, and M. G. Lagally, Surf. Sci. **219**, L551 (1989).

[21] We have observed sample degradation and the effects of Ga puddle formation at temperatures between 775 and 800 K.

[22] X.-S. Wang, R. J. Pechman, and J. H. Weaver (unpublished).

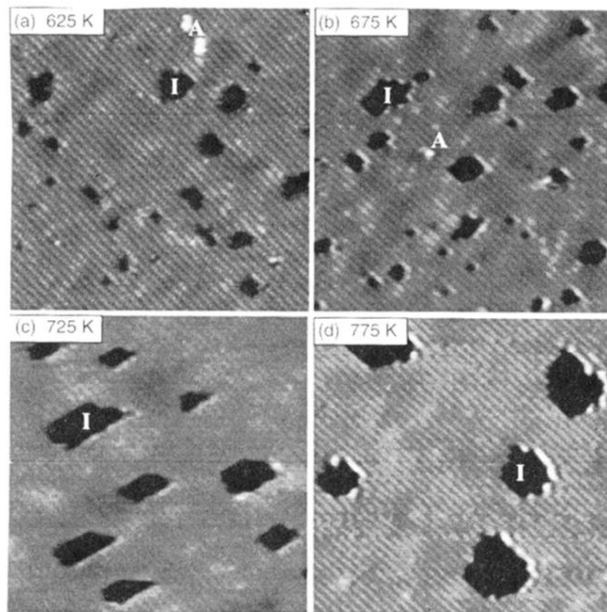

FIG. 2. 250×250-$\mathring{A}^2$ images of GaAs(110) sputtered with 300-eV Ar^+ at 3×10^{11} ions $cm^{-2} s^{-1}$ to remove ~ 0.05 ML. *I* denotes single-layer-deep vacancy islands, and *A* labels features associated with material ejected onto the surface.

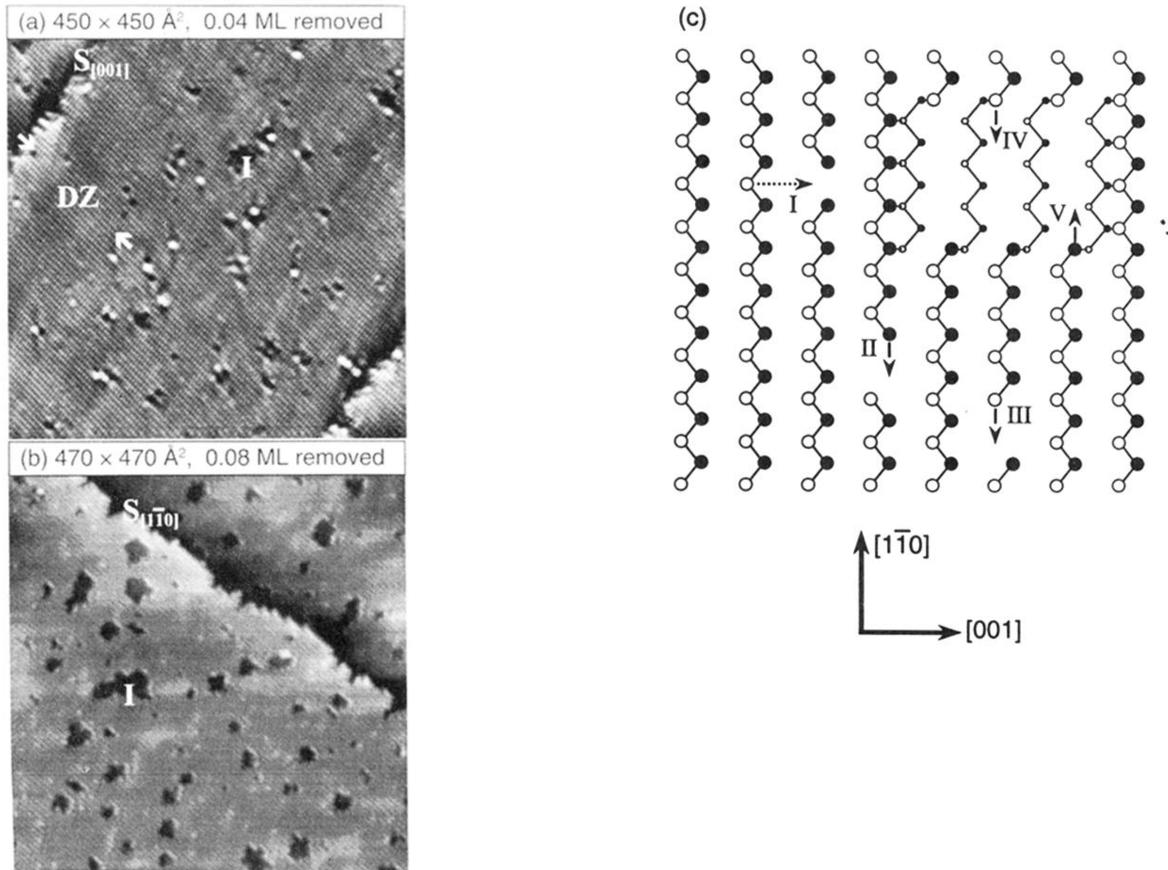

FIG. 3. (a) 450×450-Å^2 image showing a denuded zone (DZ) near a [001] step, labeled $S_{[001]}$. The island density is reduced near down-steps (upper left) but unaffected near up-steps (lower right). A typical vacancy island is indicated by I. (b) 470×470-Å^2 image of a surface sputtered to remove twice as much material as in (a). A monatomic [1$\bar{1}$0] step is seen, and no denuded zone exists. (c) Schematic representation of GaAs(110) with Ga atoms shown as filled circles and As atoms as open circles. Distinct vacancy sites are shown: a single As vacancy (V_{As}), two GaAs divacancies (V_{GaAs}), and a larger vacancy island. The zigzag row direction is indicated. Diffusion of V_{GaAs}-type defects was found to be highly anisotropic along [1$\bar{1}$0]. The arrows indicate that single atom hopping is the mechanism for net displacement.

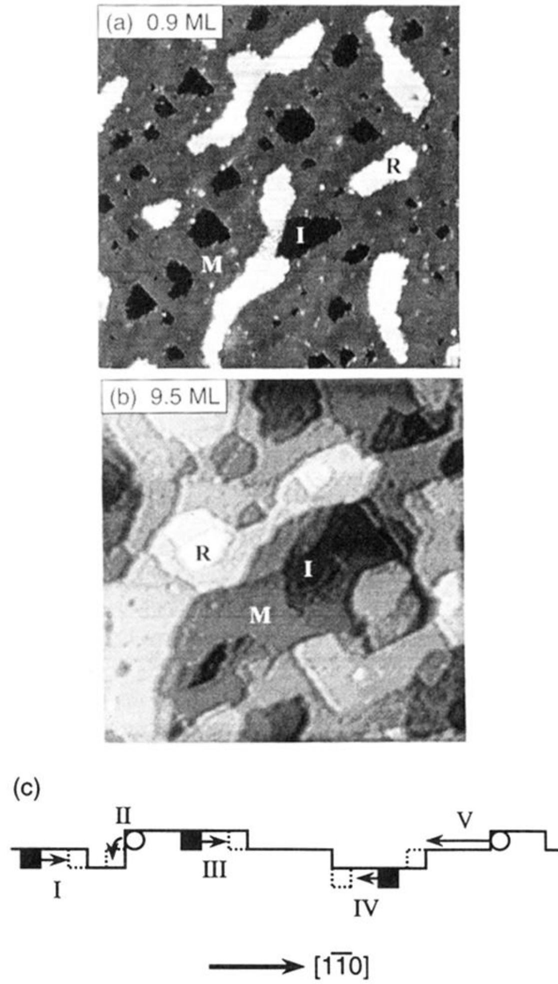

FIG. 5. 800×800-Å^2 images of GaAs(110) sputtered with 3000-eV Ar^+ at 1.9×10^{12} ions $cm^{-2}\,s^{-1}$ at 725 K to remove (a) 0.9 ML and (b) 9.5 ML. Each surface is comprised of a main layer (M), remnant layers (R), and vacancy islands (I). Three layers are exposed in (a), whereas at least eight layers are exposed in (b). (c) Surface profile during multilayer erosion depicting possible vacancy accommodation and annihilation events.

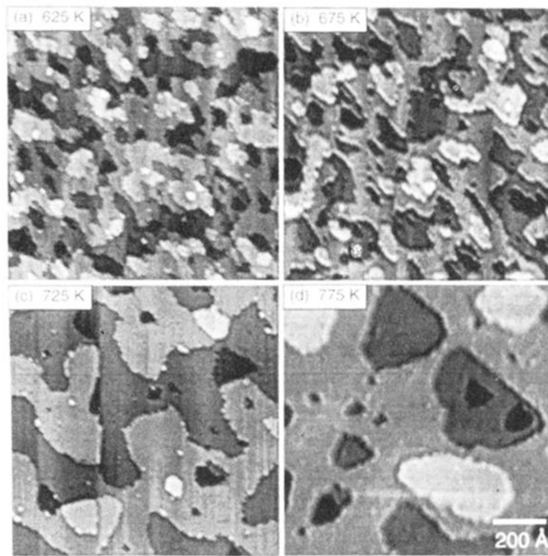

FIG. 7. 800×800-Å^2 STM images of GaAs(110) sputtered with 3000-eV Ar^+ at 1.9×10^{12} ions $cm^{-2} s^{-1}$ to remove ~ 1.5 ML. The morphology appears much smoother for the surfaces sputtered at higher temperatures, although the interface width grows in an unbounded fashion due to ineffective mass transport between layers.